Microchimica Acta 186.5 (2019): 293

**DOI:** https://doi.org/10.1007/s00604-019-3386-9

# Fluorescent C-NanoDots for rapid detection of BRCA1, CFTR and MRP3 gene mutations

Tania García-Mendiola[a,b], Cristina Garcia Elosegui[a], Iria Bravo[a,b], Félix Pariente[a,b], Alejandra Jacobo-Martin[b], Cristina Navio[b], Isabel Rodriguez[b], Reinhold Wannemacher[b] and Encarnación Lorenzo*[a,b]

[a] Departamento Química Analítica y Análisis Instrumental, Institute for Advanced Research in Chemical Sciences (IAdChem) Universidad Autónoma de Madrid, 28049 Madrid, Spain.
[b] Instituto Madrileño de Estudios Avanzados (IMDEA) Nanociencia, Faraday, 9, Campus UAM, 28049 Madrid, Spain.

## Abstract

The authors report on a fluorometric method for the rapid detection of BRCA1, CFRT and MRP3 gene mutations. These are associated with breast cancer, cystic fibrosis and autoimmune hepatitis diseases, respectively. Carbon nanodots with blue fluorescence (with excitation/emission maxima at 340/440 nm) were synthesized and characterized, and their interactions with DNA were investigated. Changes in the fluorescence intensity following interaction with ssDNA and dsDNA were used for specific DNA sequence of BRCA1, CFRT and MRP3 genes detection. The response to DNAs is linear up to 200 nM and the detection limit is 270 pM. The assay selectivity allows the detection of single gene mutations. Under optimum conditions, the assay can rapidly discriminate between wild type and mutated samples.

**Keywords:** rapid assay, Cancer, Fluorescent Carbon nanodots, DNA sensing, Mutations, Genetic diseases, Fluorescent assay.

## 1. Introduction

Common diagnostic methods of human genetic diseases are based on the detection of gene mutations. Genetic predisposition to a disease may derive from abnormal gene expressions

or from gene mutations. The usual way to detect mutations is DNA sequencing, by the classic Sanger method, but it is frequently a laborious task depending on the size of the gene and the numerous possible mutations. Hence, the development of rapid assays for the detection of specific DNA sequences or the presence of DNA mutations, based on the principle of complementary base pairing, will greatly reduce the assay time and simplify the analytical protocols. The idea is to provide assays that can perform potent molecular scans capable of identifying and analyzing changes in gene expression. This definitely will help provide less aggressive and effective therapeutic solutions and increase the chances of survival [1-6], in particular in less developed countries with limited laboratory capacities. In this sense, any cost-effective, accurate, and sensitive fluorescence assay for rapid gene mutation detection would represent an important improvement to the traditional DNA sequencing methods and an extremely valuable fast screening method. Hence, fluorescence-based systems involving different nanomaterials have been widely employed for DNA sequences detection due to the advantages of them including sensitivity, specificity and cost-effectiveness [7, 8]. In this sense, carbon nanodots (CNDs) have attracted great interest, being employed as fluorescent probes for detection of biological and environmental analytes [9, 10].

In a previous work [11] we employed carbon nanodots as a conductive nanomaterial to nanostructure screen-printed gold electrodes. It is well known that nanostructuring of the working electrode through the application of nano-sized modifiers offers attractive new features. The nanostructured electrode allows the development of an electrochemical DNA biosensor without the need of using modified DNA probes. In the present work, we wanted to go a step forward and we have taken advantage of the fluorescent properties of CNDs. First, we have synthetized a new type of CNDs using precursors specifically designed to obtain CNDs with a high quantum yield. Then, we have used these CNDs as labels of the hybridization detection to develop a rapid assay for detection of gene mutations associated with human diseases. Although based on CNDs, both strategies are completely different. Moreover, in the present work, as far as we know, is the first time that fluorescent CNDs are employed to detect specific DNA sequences and the presence of mutations, obviating in this way the need of labelling the probe or the target previously. We demonstrate the utility of the method by applying it to the detection of specific gene mutations associated to three important human diseases: 1) breast cancer gene (BRCA1) which helps suppress cancerous

cells [12]; 2) cystic fibrosis transmembrane regulator gene (CFTR) and 3) multidrug resistance protein (MRP3) gene, associated to liver diseases, such as autoimmune hepatitis.

## 2. Experimental

### 2.1. Chemicals

Citric acid 99 %, ethylene diamine, sodium phosphate and sodium chloride and all other chemicals used in this work were reagent grade quality, and were obtained from Sigma-Aldrich Co. (https://www.sigmaaldrich.com), Water was purified with a Millipore Milli-Q-System (18.2 MΩ cm) and all solutions were prepared just prior to use. Double stranded calf thymus DNA (dsDNA) was also purchased from Sigma-Aldrich Co. dsDNA stock solutions (1.0 $mg.mL^{-1}$) were prepared in 0.1 M phosphate buffer (PB) pH 7.0. The DNA solutions UV absorbance ratio ($A_{260}/A_{280}$) was about 1.9, suggesting that the DNA was free of protein [13]. Using a molar absorptivity of 6600 $M^{-1}cm^{-1}$ at 260 nm [14] the concentration in base pairs (bp) of DNA was determined. Single-stranded calf thymus DNA (ssDNA) was obtained by boiling in water capped vials containing dsDNA in 0.1 M PB pH 7.0 for 30 minutes. To prevent spontaneous renaturation, this reaction was subsequently quenched in an ice-bath. Custom-made synthetic oligonucleotides, 110-mer, from sequences of BRCA1, CFTR and MRP3 genes were supplied by Sigma-Aldrich Co. (see Table S1).

### 2.2. Experimental techniques

Fourier Transform Infrared (FTIR) spectra of pellets of KBr powder and the samples were recorded in transmission on a Bruker IFS60v Fourier-transform infrared spectrometer. Transmission electron microscopy (TEM) measurements were performed on a FEG S/TEM (Talos F200X, FEI) electron microscope. UV-vis absorption spectra were recorded on a double beam PharmaSpec UV-1700 series Shimadzu spectrophotometer operating from 200 nm to 800 nm. Fluorescence emission spectroscopy was carried out on a Cary Eclipse Varian spectrofluorimeter. Dynamic light scattering (DLS) and Zeta potential measurements were determined at 25 ºC using a Zetasizer Nano ZS instrument (Malvern Instrument Ltd., Grovewood, Worcestershire, UK). Elemental Analysis measurements were carried out using a LECO CHNS-932 system. Melting curves were performed on a UV-Visible spectrophotometer with a thermostated bath in conjunction with the spectrophotometer to

control the cuvette temperature during the measurements. The temperature inside the cuvette was determined with a platinum thermocouple. Fluorescence images were observed in an inverted microscope Axiovert200 (Zeiss) coupled to a CCD (charged-coupled device) monochrome camera and processed with Fiji-Image software. The source of illumination was a SPECTRA-X (LUMENCOR) and a 10X/0.45 Plan/Apochromat Ph 1 objective was used for detection. The excitation filter used was DAPI (395/25) and the emission was registered with a DAPI (432/36) filter.

Atomic Force Microscope (AFM) techniques were used in dynamic mode using a Nanotec Electronica system operating at room temperature in ambient conditions. The images were processed using WSxM [15]. For AFM measurements, commercial Olympus Si/N cantilevers were used with a nominal force constant of 0.75 N/m.

XPS (X ray Photoelectron Spectroscopy) measurements were performed under Ultra High Vacuum conditions (UHV, with a base pressure of $5\times10^{-10}$ mbar), using a monochromatic Al Kα line as exciting photon source for core level analysis (hν = 1486.7 eV). The emitted photoelectrons were collected in a hemispherical energy analyzer (SPHERA-U7, pass energy set to 20 eV for the XPS measurements to have a resolution of 0.6 eV) and to compensate the built up charge on the sample surface it was necessary the use of a Flood Gun (FG-500, Specs), with low energy electrons of 3 eV and 40 μA. Binding energy correction used was Si $2p_{3/2}$, 99.3 eV.

### 2.3. Procedures

Procedures for Elemental Analysis, Fourier Transform Infrared (FTIR) analysis, Atomic Force Microscopy (AFM), XPS analysis, UV-visible absorption and fluorescence emission are described in detail in Electronic Supplementary Information (ESM).

### 2.4. DNA sensing

10 μL of a 100 μM solution containing the corresponding oligonucleotide were mixed with 10 μL of a 20 μM CNDs solution and were brought to a final volume of 100 μL with 0.1M PB pH 7.0. The mixture was allowed to react for 2 h. Fluorescence of this solution was monitored at 440 nm with an excitation λ = 340 nm at room temperature. Hybridization with the target DNA was carried out by adding 20 μL of the target DNA to the oligonucleotide +

CNDs mixture, bringing it to a final volume of 100 µL with 0.1 M PB pH 7.0 + 0.4 M NaCl and heating it for 1 h at 40 ºC. After cooling to room temperature, fluorescence was monitored at the same excitation wavelength.

## 3. Results and discussion

### 3.1. Choice of Materials.

Great efforts have been focused on the synthesis of non-toxic fluorescent nanomaterials as an alternative to the well-known semiconductor quantum dots containing toxic heavy metals. Carbon nanodots (CNDs) are recently discovered C-based nanomaterials that comprise discrete, quasispherical nanoparticles with sizes below 10 nm [9, 16-21]. These C nanomaterials can be produced easily from a wide range of raw materials by methods that do not require scarce elements or stringent, intricate, tedious, costly, or inefficient preparation steps [20, 22]. Moreover, they present robust chemical inertness, high solubility in aqueous media and, similar to quantum dots (QDs), good photostability [16, 23, 24], but they excel by their high biocompatibility, due to the absence of toxic metal ions. They can also be excellent sensing platforms for DNA, a topic still insufficiently explored. The DNA sensing method would be based on changes in CNDs fluorescence intensity after interaction with single or double-stranded DNA. Compared to other fluorescent probes used for gene mutation detection, such as Ag nanoclusters [25] or a iridium (III) based complex [26], CNDs present robust chemical inertness, high solubility in aqueous media, high biocompatibility, due to the absence of toxic metal ions and can be produced easily from a wide range of raw materials.

### 3.2. Synthesis and characterization of Carbon Nanodots (CNDs)

We have synthetized highly fluorescent CNDs by using citric acid and ethylenediamine as precursors by a hydrothermal method [27] as described in the Electronic Supplementary Information (ESM) and depicted in Figure S1. The obtained CNDs were characterized by different techniques. From TEM (Figure S1) we concluded that CNDs reveal a spherical morphology with diameters distributed in a narrow range (2-6 nm) and an average value of 4.1 ± 0.3 nm. FFT analysis determined a spacing of planes (Figure 1B and C) of 2.1 Å, which is characteristic of the CNDs (100) plane. From AFM measurements (Electronic

Supplementary Information Figure S2) a homogeneous distribution of CNDs is observed. From the histogram and profile of the magnified image (Electronic Supplementary Information Figure S2 C and D) an average height of 5.5 ± 1.1 nm and the large extent in size in the xy- direction can be explained by the presence of aggregates. Elemental analysis indicates that CNDs contain: 40.5% C, 4.8% N and 7.2% H.

XPS was found to be useful in terms of deriving structural information for CNDs. The contributions stemming from the core levels of C1s, N1s and O1s were noted. Deconvolution of the C1s core-level region of CNDs points to three species with binding energies of 286.0 (C-H and C-C), 287.84 (C-NH and C-OH) and 289.6 eV (C=O, N-C=O, O=C-OH) (Electronic Supplementary Information Figure S3). The fit of N1s line of CNDs points to two species with binding energies of 402.6 (C-N) and 401.2 eV (O=C-NH). From XPS, an elemental composition of 61.2% C, 10.5% N, 28.3% O was derived. The C/N ratio suggests a slight surface enrichment of N.

FTIR spectroscopy was also used to investigate the functional groups of the synthesized CNDs. FTIR spectrum (Figure 1A) exhibits the characteristic stretching band of hydroxide at 3417 $cm^{-1}$ besides stretching vibrations of C=O at 1711 $cm^{-1}$ and the –N-H stretching peak at 1621 $cm^{-1}$. Bands at 1366 $cm^{-1}$ and 1189 $cm^{-1}$ are assigned to the stretching vibrations of C-H [27], confirming the results obtained about the functional groups of the CNDs by XPS.

The UV-vis absorption spectrum in water (Figure 1B) shows a broad peak around 343 nm, ascribed to n-π* transitions of C=O bonds [28]. The fluorescence spectrum when excited at 340 nm shows an emission band with a peak at 440 nm. By changing the excitation wavelength from 320 to 400 nm ($\Delta\lambda ex$ = 80 nm), the emission maximum only decreases in intensity as $\lambda ex$ moves away from the absorption maximum but does not shift its position. The full width at half maximum obtained was 80 ± 2 nm confirming a homogeneous ensemble of CNDs. In all further experiments, excitation and emission wavelengths of 340 and 440 nm, respectively, were used.

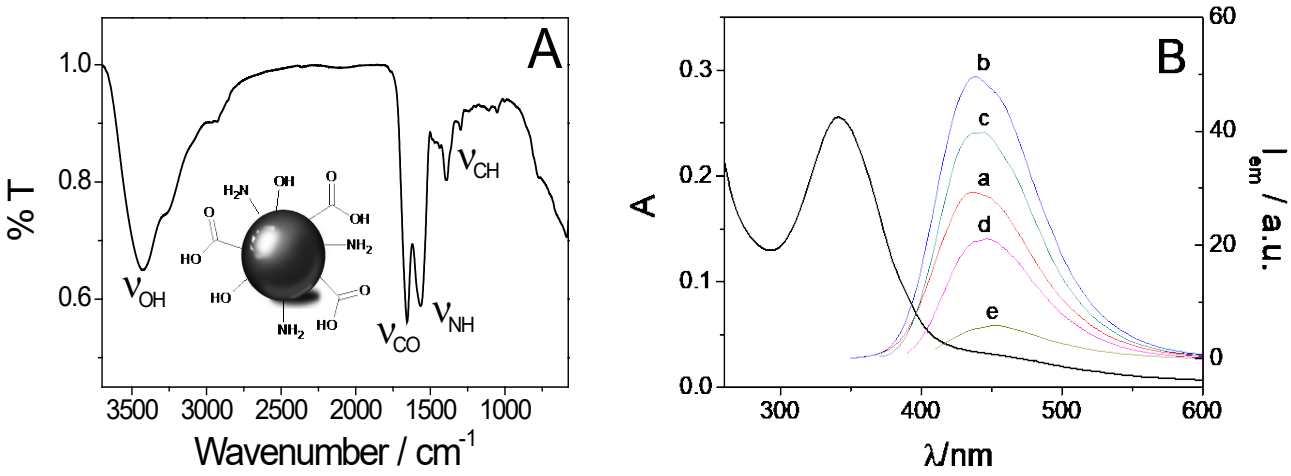


Figure 1. A) FTIR spectrum of the synthesized CNDs. B) Absorbance and Fluorescence emission spectra of a 2.0 μM CNDs in water. Fluorescence emission spectra at different excitation wavelengths: (a) 320 nm, (b) 340 nm, (c) 360 nm, (d) 380 nm and (e) 400 nm.

The CNDs were stable over at least 4 months with only minor changes in the fluorescence spectral profiles (data not shown). This greatly aids in their commercial use for different applications such as (bio)sensing or bioimaging. The CNDs quantum yield was calculated to be 30%.

The pH study demonstrates that while the absorption does not change upon pH variation, emission intensities decrease in a solution of high or low pH, but remain constant in a solution of pH 5-8 (Electronic Supplementary Information, Figure S4). Hence, the fluorescence of the nanomaterial does not change appreciably within the physiological medium and therefore allows sensing of other factors. In particular, we used this for DNA sensing.

### 3.2. CNDs-DNA interaction

In order to analyze the interaction of CNDs with DNA, the melting temperature $T_m$ in the absence and in the presence of CNDs was compared (Electronic Supplementary Information, Figure S5). In the presence of CNDs, $T_m$ exhibits an increase of 12 ± 2 ºC. The $T_m$ serves as a simple although powerful tool for determination of the helix stability after interaction with a molecule [29]. Such a study is able to provide insight into the conformational changes of DNA in presence of an interacting compound and also information about the interaction

strength. When a given molecule interacts strongly with dsDNA, the stability of the double-helix improves, and as a result, the melting temperature $T_m$ increases by about 5-8 ºC [29]. No interaction causes no obvious increase in $T_m$ [30]. Hence, our result is consistent with a strong interaction.

DLS, Zeta potential and FTIR were used to assess the interaction. A detailed description of the procedures followed in these studies is provided in the Experimental Section. Particle sizes determined by DLS of dsDNA-CNDs nanohybrid and dsDNA were 1264 and 514.8 nm, respectively. The increase in the size is concordant with the formation of aggregates. Such aggregates are also revealed by TEM (Electronic Supplementary Information Figure S6) and phosphorus from the DNA is identified by EDX. The Zeta potential was found to be -40.0 mV in both cases, which agrees well with the presence of phosphate groups in the DNA backbone that remain unaffected after interaction with CNDs. The FTIR spectrum of the nanohybrid shows only the characteristic bands of both the DNA and CNDs (Electronic Supplementary Information, Figure S7). This result suggests that the interaction between CNDs and DNA is due to H-bonding and π-π interactions.

Fluorescence microscopy confirms the interaction of CNDs with DNA. Figure 2 shows the optical and fluorescence micrographs (obtained with excitation from 375 to 420 nm and emission from 396 to 468 nm) of dsDNA, ssDNA-CNDs, dsDNA-CNDs and CNDs samples. As can be observed, dsDNA-CNDs nanohybrid (G) shows fluorescence from CNDs, since DNA by itself does not present fluorescence under the experimental conditions employed (see control image (E)). On the contrary, CNDs aggregates strongly fluoresce (H). The micrograph of ssDNA-CNDs sample (F) presents much lower fluorescence than the one of dsDNA-CNDs (G). These results suggest that CNDs interact preferably with dsDNA, probably because in this case besides to the H-bonding and π-π interactions, CNDs can bind to dsDNA by insertion in the major grooves.

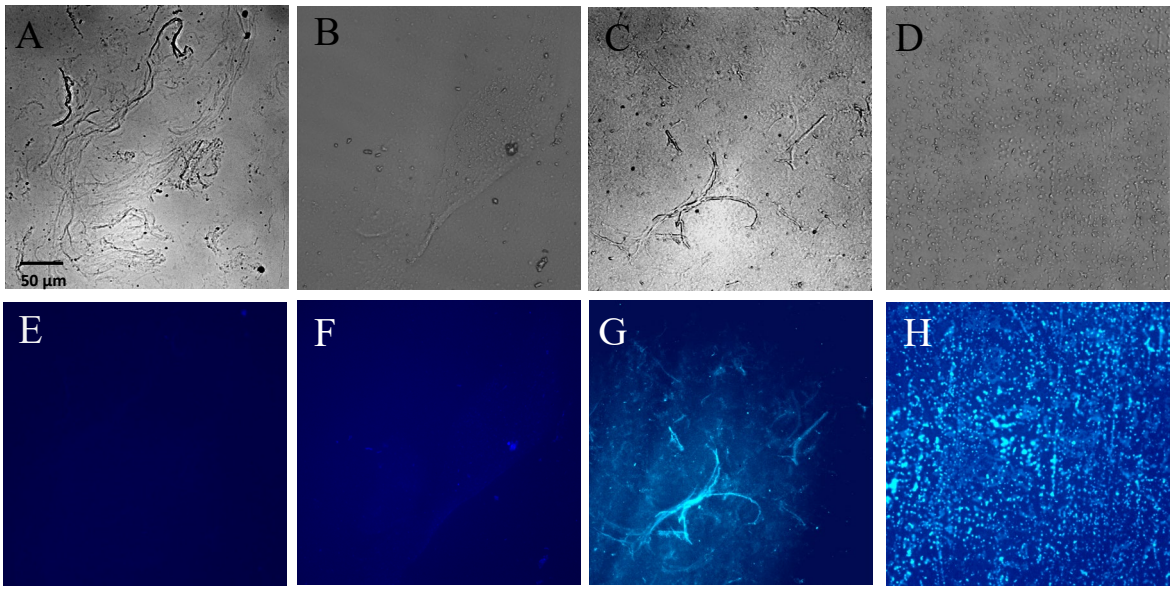


Figure 2. Optical micrographs (top line) and fluorescence micrographs (bottom line) of dsDNA (A, E), ssDNA-CNDs (B, F) or dsDNA-CNDs (C, G) nanohybrid samples and CNDs (D, H).

We next investigated whether the fluorescence of CNDs depends on the presence of DNA in solution, which is important for CNDs to be used as DNA sensing platforms. Figure 3A shows the fluorescence spectra of CNDs in the absence and in the presence of increasing amounts of dsDNA. Excitation at 340 nm, in the absence of dsDNA, results in the characteristic fluorescence emission band at 440 nm. The addition of dsDNA gives rise to a significant gradual increase of the emission intensity with no evident shift in the emission maximum. The quantum yield increased from 30 % to 60 % at 5 µM dsDNA. The interaction mode, however, is not fully established and work is in progress to elucidate it. Most likely, as it happens with some molecules [31], upon noncovalent binding of CNDs to DNA the non-radiative decay is less efficient, resulting in fluorescent enhancement. CNDs bounds to the DNA along the backbone by H-bonding and π–π interactions. The binding constant ($K_b$) was calculated to be $1.7\pm0.3 \times 10^4$ $M^{-1}$. This value is similar to those reported for some compounds that interact strongly with DNA [32].

As can be seen in Figure 3B, CNDs fluorescence is much less affected by the presence of ssDNA in solution, confirming that this nanomaterial interacts to a different extent with ds and ssDNA. In the case of the former there is a new component in the interaction due to the insertion of CNDs in the major grooves.

Iodide is a well-known quencher for many fluorophores due to enhancement of intersystem crossing. The quenching effect can be used to determine whether the fluorophores are exposed to KI [33]. In our case, the presence of 5 mM iodide causes only a small decrease in the CNDs fluorescence (Electronic Supplementary Information, Figure S8). This suggests that the main fluorescence emission seems to come from fluorophores inside the CNDs and, therefore, iodide cannot reach them. In presence of DNA, the fluorescence is even less affected by the iodide. This is probably due to the Coulomb repulsion between iodide and negatively charged DNA backbone phosphates.

### 3.3. DNA sensing

Fluorescence spectroscopy and microscopy studies confirmed that, as some small molecules, CNDs interact to a different extent with dsDNA and ssDNA. We therefore explored if it can be employed for DNA sensing by analyzing a 100-mer synthetic sequence of BRCA1 gene. The method is based on changes in the fluorescence of the capture DNA probe (a sequence fully complementary to the target DNA sequence)-CNDs nanohybrid after hybridization with the target DNA.

Figure 3C shows that the fluorescence of CNDs practically does not change after incubation with the DNA capture probe, in order to form the DNA probe-CNDs nanohybrid. However, after hybridization of the nanohybrid with the target (a sequence of BRCA1 totally complementary to the capture probe) a significant enhancement in the emission is observed, while a very small change is noted for a non-complementary sequence used as control. The fluorescence emission shows excellent correlation with the amount of the target sequence up to 200 nM (Figure 3D) and a reproducibility of 95 %. The detection limit was calculated as 270 pM (according to the 3 x $S_b$. $m^{-1}$ criteria, where $S_b$ corresponds to the standard deviation (n = 6) for measurements made with non-target DNA and m is the slope of the calibration plot. The detection limit obtained in the present work is comparable or even better than the

reported in the literature for gene mutation detection using similar nanomaterial-based luminescent methods (see Electronic Supplementary Information Table S2).

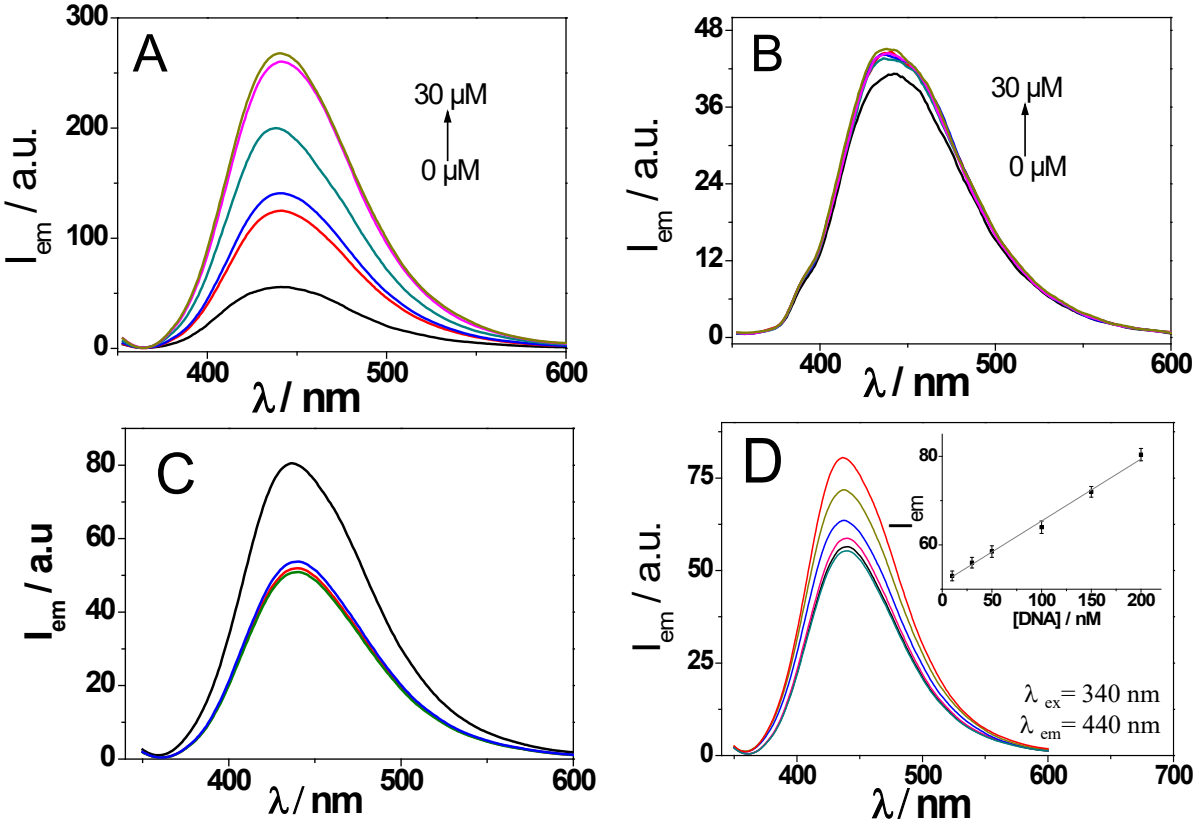


Figure 3. Emission spectra of 2.0 µM CNDs in 0.1 M PB pH 7.0, in absence (black curve) and presence (colored curves) of dsDNA (A) and ssDNA (B). Fluorescence spectra of CNDs before (green curve) and after incubation with the DNA capture probe (red curve) and after addition of the target, a sequence of BRCA1 totally complementary to the capture probe (black curve) or a non-complementary sequence (blue curve) (C). Fluorescence spectra of DNAprobe-CNDs nanohybrid after hybridization with increasing concentrations of the BRCA1 gene sequence (D). Inset: Calibration plot constructed with the DNA assay of the BRCA1 gene sequence.

### 3.4. Gene mutation detection

The selectivity of the assay was evaluated by detecting partially complementary sequences based on gene mutations associated with different human diseases. As is depicted in the Scheme of Figure 4, the mutation detection relies on the formation of the nanohybrid between the corresponding DNA capture probe and CNDs and the comparison between the signals (fluorescence) obtained before and after hybridization with the totally complementary Wild Type sequence (WT) or the sequence carrying the mutation (MUT). We have analyzed mutations consisting on a single mismatch from BRCA1 and MRP3 gene associated to breast cancer, and autoimmune hepatitis, respectively; and one consisting on three-base deletion from CFTR gene associated to cystic fibrosis (corresponding sequences are summarized in Electronic Supplementary Information, Table S1). Figure 4 A, B and C show that the native fluorescence of the CNDs is only slightly affected after their incubation with the different capture DNA probes to form the corresponding DNA probe-CNDs nanohybrid. However, after hybridization of each DNA probe-CNDs nanohybrid with its WT sequence the fluorescence emission increases from 50 a.u. to above 75 a.u (with a maximum error of 1.8 a.u). Hybridization with the MUT sequence gives rise to a lower enhancement of around 10 a.u. (with a maximum error of 1.5 a.u) and with a fully non-complementary sequence causes no effect. Given the small error associated to each measurement, we can conclude that the method can clearly discriminate between WT and MUT sequences allowing the detection of the different gene mutations as is presented in Figure 4D. Moreover, it is worth to note that the assay is sensitive to the grade of non-complementarity of the target sequence. In the case of CFTR gene, the difference in the response between WT and MUT is higher than in the other cases. In this case, the mutation relies on a three-base deletion causing the loss of a phenylalanine residue. However, in the case of MRP3 or BRCA1 the mutation consists in a single nucleotide polymorphism (SNP).

We anticipate the assay will find broad application to the identification of specific DNA sequences and gene alterations. Although as a prove of concept we have demonstrated the applicability of the assay on synthetic samples, work is in progress employing clinical samples. The limitation in this case consists on the genomic DNA must be previously extracted from biomatter and amplified by PCR.

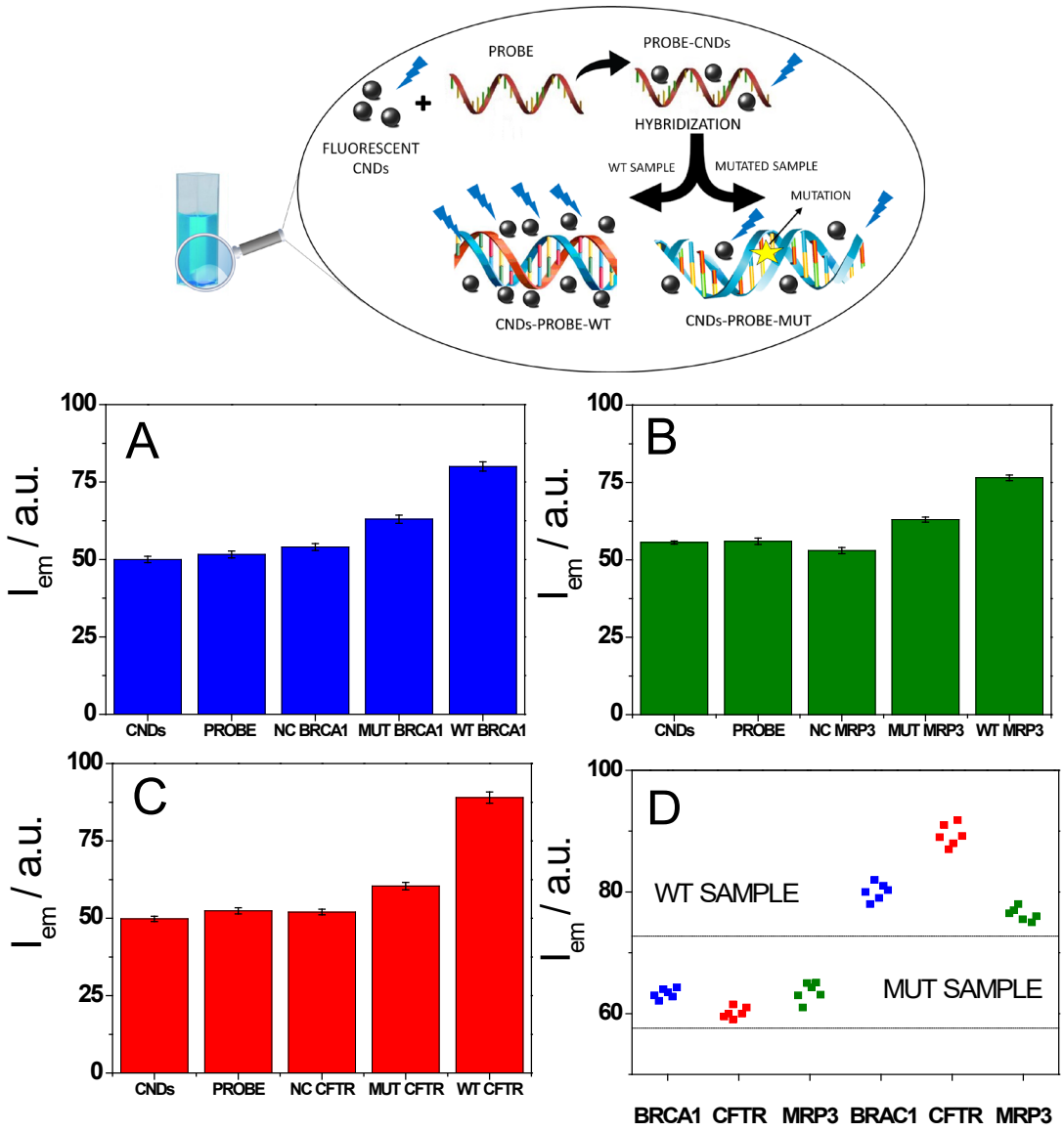


Figure 4. Scheme followed for gene mutation detection. Bar diagrams of CNDs fluorescence emission before (CNDs), after interaction with the probe (PROBE) and after hybridization with: fully complementary (WT), mutated (MUT) or non-complementary (NC) sequences from BRCA1 (A), CFTR (B) and MRP3 (C) gene associated to breast cancer, cystic fibrosis and autoimmune hepatitis, respectively. Summary plot of the signals obtained for all the samples measured (D).

## 4. Conclusions

In summary, for the first time we have employed the interaction of carbon nanodots (CNDs) and DNA to develop a novel and effective assay for the rapid detection of gene mutations. Fluorescent CNDs were synthesized by simple hydrothermal carbonization of ethylendiamine and citric acid. Different techniques confirm that the synthesized CNDs interact to a different extent with dsDNA and ssDNA, resulting in different fluorescent response. Hence, they can be employed as a rapid and label-free assay for detection of not only the hybridization event and DNA sensing, but also for gene mutation detection. Although three genes were used as the triggering target for the assay demonstration, our system in principle can be extended to the detection of other genes. These applications can be of great interest for faster assessment, better management and improved treatment of cancer and other important diseases. Compared to other methods reported for the detection of gene mutation, our method is highly simple and rapid, and uses unmodified oligonucleotides, thus avoiding the relatively high cost for covalent labeling, like the methods that use fluorescent metal-based complexes, but the synthesis of CNDs is easy. They can be synthetized from very common row and low-cost materials. The method has been applied to gene mutations consisting on a single mismatch oligonucleotide or a deletion, but one would expect that other type of DNA mutation can be also detected.

## Acknowledgements

This work has been supported by the Comunidad Autónoma de Madrid projects (NANOAVANSENS, S2013/MIT-3029 and MAD2D-CM Program, S2013/MIT-3007) and Spanish Ministerio de Economía, Industria y Competitividad through projects: CTQ2015-71955-REDT (ELECTROBIONET), CTQ2014-53334-C2-1-R. and MAT2015-71879-P. We thank the Confocal Microscopy and Flow Cytometry Services of CBMSO.

## References

1. Cattrall RW (1997) Chemical Sensors, Chemistry Primers. Oxford University Press, Oxford UK

2. Mickelsen SR (1996) Electrochemical biosensors for DNA sequence detection. Electroanalysis 8:15-19

3. Palecek E, Fojta M, Tomschik M, Wang J (1998) Electrochemical biosensors for DNA hybridization and DNA damage. Biosens Bioelectron 13:621-628

4. Wang J (2006) Electrochemical biosensors: Towards point-of-care cancer diagnostics. Biosens Bioelectron 21:1887-1892

5. Miao P, Liu L, Nie YJ, Li GX (2009) An electrochemical sensing strategy for ultrasensitive detection of glutathione by using two gold electrodes and two complementary oligonucleotides. Biosens Bioelectron 24:3347-3351

6. Wan Y, Zhang J, Liu G, Pan D, Wang LH, Song SP, Fan CH (2009) Ligase-based multiple DNA analysis by using an electrochemical sensor array. Biosens Bioelectron 24:1209-1212

7. Ma H, Li Z, Xue N, Cheng Z, Miao X (2018) A gold nanoparticle based fluorescent probe for simultaneous recognition of single-stranded DNA and double-stranded DNA. Microchim Acta 185:93

8. Qian ZS, Shan XY, Chai LJ, Ma JJ, Chen JR, Feng H (2014) A universal fluorescence sensing strategy based on biocompatible graphene quantum dots and graphene oxide for the detection of DNA. Nanoscale 6:5671-5674

9. Li HT, Kang ZH, Liu Y, Lee ST (2012) Carbon nanodots: synthesis, properties and applications. J Mater Chem 22:24230-24253

10. Zhong D, Zhuo Y, Feng YJ, Yang XM (2015) Employing carbon dots modified with vancomycin for assaying Gram-positive bacteria like Staphylococcus aureus. Biosens Bioelectron 74:546-553

11. García-Mendiola T, Bravo I, López-Moreno JM, Pariente F, Wannemacher R, Weber K, Popp J, Lorenzo E (2018) Carbon nanodots based biosensors for gene mutation detection. Sens Actuators B: Chem 256:226-233

12. D'Andrea E, Marzuillo C, De Vito C, Di Marco M, Pitini E, Vacchio MR, Villari P (2016) Which BRCA genetic testing programs are ready for implementation in health care? A systematic review of economic evaluations. Genet Med 18:1171-1180

13. Marmur J (1961) Procedure for Isolation of Deoxyribonucleic Acid from Micro-organisms. J Mol Biol 3:208-218

14. Doty P, Rice SA (1955) The Denaturation of Desoxypentose Nucleic Acid. Biochim Biophys Acta 16:446-448

15. Horcas I, Fernández R, Gómez-Rodríguez JM, Colchero J, Gómez-Herrero J, Baro AM (2007) WSXM: A software for scanning probe microscopy and a tool for nanotechnology. Rev Sci Instrum 78:013705

16. Baker SN, Baker GA (2010) Luminescent Carbon Nanodots: Emergent Nanolights. Angew Chem Int Ed 49:6726-6744

17. Shen JH, Zhu YH, Yang XL, Li CZ (2012) Graphene quantum dots: emergent nanolights for bioimaging, sensors, catalysis and photovoltaic devices. Chem Commun 48:3686-3699

18. Zhang ZP, Zhang J, Chen N, Qu LT (2012) Graphene quantum dots: an emerging material for energy-related applications and beyond. Energ Environ Sci 5:8869-8890

19. Zhu SJ, Tang SJ, Zhang JH, Yang B (2012) Control the size and surface chemistry of graphene for the rising fluorescent materials. Chem Commun 48:4527-4539

20. Cao L, Meziani MJ, Sahu S, Sun YP (2013) Photoluminescence Properties of Graphene versus Other Carbon Nanomaterials. Acc Chem Res 46:171-180

21. Li LL, Wu GH, Yang GH, Peng J, Zhao JW, Zhu JJ (2013) Focusing on luminescent graphene quantum dots: current status and future perspectives. Nanoscale 5:4015-4039

22. Li LL, Ji J, Fei R, Wang CZ, Lu Q, Zhang JR, Jiang LP, Zhu JJ (2012) A Facile Microwave Avenue to Electrochemiluminescent Two-Color Graphene Quantum Dots. Adv Funct Mater 22:2971-2979

23. Wang YF, Hu AG (2014) Carbon quantum dots: synthesis, properties and applications. J Mater Chem C 2:6921-6939

24. Chen L, Han HY (2014) Recent advances in the use of near-infrared quantum dots as optical probes for bioanalytical, imaging and solar cell application. Microchim Acta 181:1485-1495

25. Borghei Y, Hosseini M, Ganjali MR (2017) Detection of large deletion in human BRCA1 gene in human breast carcinoma MCF-7 cells by using DNA-Silver Nanoclusters. Methods Appl Fluoresc 6:015001

26. He H, Chan DS, Leung C, Ma D (2012) A highly selective G-quadruplex-based luminescent switch-on probe for the detection of gene deletion. Chem Commun 48:9462-9464

27. Zhu SJ, Meng QN, Wang L, Zhang JH, Song YB, Jin H, Zhang K, Sun HC, Wang HY, Yang B (2013) Highly Photoluminescent Carbon Dots for Multicolor Patterning, Sensors, and Bioimaging. Angew Chem Int Ed 52:3953-3957

28. Wen Z, Yin X (2016) Excitation-independent carbon dots, from photoluminescence mechanism to single-color application. RSC Adv 6:27829-27835

29. Mergny JL, Duval-Valentin G, Nguyen CH, Perrouault L, Faucon B, Rougée M, Montenay-Garestier T, Bisagni E, Hélène C (1992) Triple Helix-Specific Ligands. Science 256:1681

30. Kumar CV, Turner RS, Asuncion EH (1993) Groove binding of a styrylcyanine dye to the DNA double helix: the salt effect. J Photochem Photobiol A Chem 74:231-238

31. Cosa G, Focsaneanu K-, McLean JRN, McNamee JP, Scaiano JC (2001) Photophysical Properties of Fluorescent DNA-dyes Bound to Single- and Double-stranded DNA in Aqueous Buffered Solution. Photochem Photobiol 73:585-599

32. Heli H, Moosavi-Movahedi AA, Jabbari A, Ahmad F (2007) An electrochemical study of safranin O binding to DNA at the surface. J Solid State Electrochem 11:593-599

33. Lakowicz JR (2006) Principles of Fluorescence Spectroscopy. Springer